Label Free Biomolecule Detection in Physiological Solutions with Enhanced Sensitivity using Graphene Nanogrids FET Biosensor

R.Ray, J.Basu, W.A. Gazi, N.Samanta, K.Bhattacharyya and C.RoyChaudhuri *Senior Member, IEEE*

***Abstract*— Recently, graphene nanogrid sensor has been reported to be capable of sub-femtomolar sensing of Hepatitis B (Hep-B) surface antigen in buffer. However, for such low concentration of Hep-B in serum, it has been observed during real time operation, that there is an overlap of around 50% in the drain-source current sensitivity values between different concentrations of the target biomolecule, in the range of 0.1 fM to 100 fM. This has been attributed to the fact that the concentration of non-specific antigen in serum being significantly higher than that of the target antigen, there is a considerable deviation in the number of captured target antigen for the same concentration. Further, this degree of overlap varies from one set to another set of sensor depending on the statistical variations in the sensor fabrication process. This phenomenon challenges the quantification of target antigen for ultralow limit in physiological analyte. In this paper, we introduce probabilistic neural network (PNN) for quantification of Hep-B down to 0.1 fM in serum using graphene nanogrids field effect transistor (FET) biosensor. The sensor has been operated in heterodyne mode in the frequency range of 100 kHz to 1 MHz applied between drain and source to overcome the problem of Debye screening effect. The application of PNN limits the quantification error within 10% in the range of 0.1 fM to 100 fM in contrast to 77% and 66% using polynomial fit and static neural network models respectively. Further, the proposed methodology lowers the detection limit of Hep-B in serum by more than three orders of magnitude compared to the state-of the art real-time, label free sensors.**

***Index Terms*—graphene nanogrid, field effect transistor biosensor, physiological analyte, sub-femtomolar, probabilistic neural network**

Manuscript submitted on 11th April 2018. This work has been financially supported by Visveswaraya Young Faculty Research Award,IMPRINT project, Govt. of India. One of the authors, Ms. Jayeeta Basu receives her fellowship from the Institute. The corresponding author of this paper is C.RoyChaudhuri.

R.Ray, J.Basu and N.Samanta is with the Electronics and Telecommunication Engineering Department, IIEST, Shibpur, Howrah 711103, India.

W.A.Gazi is with Qualcomm Technologies,Bangalore, India

K.Bhattacharyya is with the Department of Medical Sciences, JJT University, Rajasthan, India

C. RoyChaudhuri is with the Electronics and Telecommunication Engineering Department and Center for Healthcare Science and Technology, IIEST, Shibpur, Howrah 711103, India (email: chirosreepram@yahoo.com).

I. Introduction

DETECTION of biomolecules electronically by conductance, impedance and amperometric measurements have been extensively investigated. The various nanostructures fabricated for the purpose includes nanowires [1],nanoribbons [2], ordered and random nanopores [3], nanotubes [4], nanorods [5] and nanoparticles [6]. The substrates commonly deployed for realizing these nanostructures include silicon and its oxide, indium oxide, graphene, carbon nanotubes, anodized alumina, zinc oxide and various polymers[1-7]. Nanostructured substrate not only improves the binding efficiency of the analyte due to large surface area to volume ratio but also shows a possible catalytic effect in the diffusion of the analyte molecules within the nanopores[7]. In this aspect, the 3D configurations of the nanostructures are expected to be significantly more sensitive than their 2D counterparts, owing to larger surface area to volume ratio and increased diffusion flux [8]. Graphene being an intrinsically zero band gap material, its band gap can be tailored significantly by applying external electric field or by surface adsorption of charged biomolecules, resulting in a significant modulation of the transconductance. This feature enables superior performance with FET configuration. Thus, in particular,3D graphene has been recently explored [9-12] in the form of nanorods, nanowalls and nanogrids for ultrasensitive detection of various biomolecules like proteins, DNA, virus and others. For example, it has been reported that reduced graphene nanowalls, fabricated by electrophoretic deposition on graphite electrode from a suspension containing Mg^{2+}-graphene oxide nanosheets results in ultra-high resolution electrochemical biosensor for detection of four bases of DNA using differential pulse voltammetry [13]. This has been possible due to increased edge defects and high surface area to volume ratio. Further, the authors have fabricated smooth 3D graphene nanogrids by a reliable and scalable chemical method which has resulted in attomolar sensitivity in a FET configuration [12]. The improved sensitivity was attributed to the combined effects of insignificant line edges, quantum dot like transport behaviors and improved interaction of the biomolecules within the nanopores due to the concave curvature. However, there are

This article has been accepted for publication in a future issue of this journal, but has not been fully edited. Content may change prior to final publication. Citation information: DOI 10.1109/TNB.2018.2863734, IEEE Transactions on NanoBioscience

only few reports on investigating graphene FET biosensors in physiological solutions.

For sensing in physiological solutions, one of the major challenges is overcoming the Debye screening effect. This problem has been addressed by two methods: applying a high frequency signal between the source and drain which results in the breakdown of the electric-double-layer (EDL) near the surface of the FET channel, due to fast switching of the direction of the applied bias, leading to deeper penetration of the electric potential of the target protein and another technique is coating the channel surface with polyethylene glycol which increases the effective screening length [14-16]. However, the intrinsic transconductance decreases in the latter due to increased thickness of the immobilized layer. These techniques have been applied in graphene field effect transistors. Gao and colleagues have reported sensing of prostate specific antigen in physiological solutions using graphene FET biosensors [17] but the detection limit is in nM range. Graphene sensor has been used for detection of Zika virus, protein biomarkers and lead ions in serum but the detection limit is either in nanomolars or few hundreds of femtomolars [18-20]. The low sensitivity may be attributed to the 2D nature of the graphene substrate. It is expected that 3D graphene nanostructures will enable few femtomolar sensing of biomolecules in serum. But for real time quantification of biomolecules in serum down to few femtomolars, the problem may be non-trivial. There is a possibility of overlap of the drain-source current sensitivity values between different concentration of the target biomolecule, especially near the lower range since in presence of serum containing large concentration of non-target molecule, there may be significant deviations in the number of target antigen captured and hence the sensitivity for a fixed concentration of the target. Again, this degree of overlap can vary from one set to another set of sensor depending on the statistical variations in the sensor fabrication process. To address this multi-level uncertainty, it will be necessary to process the output by signal processing schemes incorporating probabilistic features.

Signal processing tools like fuzzy logic, neural networks, progressive least square fitting and others have been applied by various researchers in chemical and biological sensors in practical settings but these sensors mostly involved washing or recovery steps which reduced the uncertainties in the electrical outputs [21-26]. Probabilistic algorithms like probabilistic fuzzy logic (PFL) has been applied by other researchers to model stochastic biological phenomena with uncertain kinetic parameters and for cancer network analysis [27-29]. Probabilistic neural network (PNN) has been successfully deployed in pathogen classification by incorporating the uncertainties in the data [30-31].Further, it has been indicated that PNN results in lower quantification errors than PFL.But such probabilistic schemes have not been deployed previously in biochemical sensors.

In this paper, we introduce for the first time probabilistic neural network for real time quantification of target antigen down to 0.1 fM concentration in serum using graphene nanogrids FET based transconductance biosensors. Hep-B surface antigen has been selected as the target molecule. The drain source current sensitivities have been analyzed by three methods for quantification to strengthen the justification for application of PNN. The performance of the PNN processed graphene nanogrid FET sensor has been compared with the state-of-the art reports.

II. Materials and Methods

A. *Fabrication of graphene nanogrid FET biosensor chip*

Graphene nanogrid structure has been fabricated using a two step process. Firstly nanoporous silicon oxide (NPSO) substrate has been developed by anodic etching of p-type <100> silicon wafers of 10–20 Ω cm resistivity in a double pond electrochemical bath for 30 min under a constant current source with an electrolyte mixture of hydrofluoric acid (HF) (48 wt%) and dimethyl sulfoxide (DMSO) in the ratio of 1:9 by volume. The structure has been thermally oxidized using a dry-wet-dry sequence in an oxidation furnace for1 h at 900°C to obtain pores with 30 nm diameter (*d)* and 100 nm length (*l)*. Secondly, graphene has been deposited on nanoporous silicon oxide substrate by electrophoretic deposition (EPD) method.

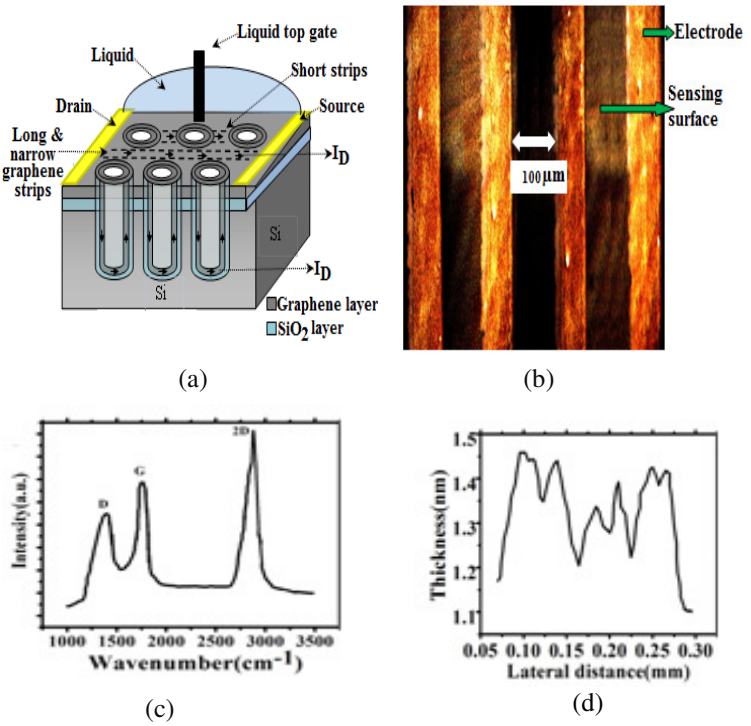

Fig.1(a) Schematic of graphene nanogrid sensor (b) Optical image of the sensor (c) Raman spectroscopy and (d) surface profilometry of graphene

Interdigited metal electrodes have been fabricated on the substrate for EPD of graphene with aluminium by screen printing method which has been next cured at 750°C for 1 min. The width of the electrodes is 60 µm and spacing between two consecutive fingers of each electrode is 100µm. This has been followed by evaporation of gold metal which improves the longevity of the sensor. The electrodes have been connected with function generator and the prepared colloidal graphene solution has been pipetted onto the substrate so that the droplet of the solution should be covering

This article has been accepted for publication in a future issue of this journal, but has not been fully edited. Content may change prior to final publication. Citation information: DOI 10.1109/TNB.2018.2863734, IEEE Transactions on NanoBioscience

the electrodes. Then a sinusoidal voltage (peak to peak 19.5 V) has been applied for 60 s. The graphene deposited substrate has been heated at 75 °C for 2 min for increasing the adhesion between graphene and the substrate. The aforesaid fabrication results in a nanogrid structure with long and narrow graphene strips alternating with series combination of short and narrow strips on planar regions and within pores, the schematic of which is shown in Fig.1a. An optical image of a section of the sensor with the interdigitated electrodes is shown in Fig.1b. The Raman spectroscopy and surface profilometry of graphene is indicated in Fig.1c and 1d. It has been observed from Fig.1c that the G peak is higher than D peak which indicates low defect density. The presence of prominent 2D peak in Fig.1c points towards the bilayer nature of graphene.

B. Immobilization Process

For immobilization of anti Hep-B monoclonal antibody, (procured from Sigma Aldrich, St. Louis, MO, USA) the graphene nanogrid structure has been treated with 25% glutaraldehyde aqueous solutions (procured from Sigma Aldrich) for 4 h. Glutaraldehyde acts as a crosslinker, which helps the antibody bind covalently with the substrate by activating the negatively charged carboxylic groups of graphene. After treatment, the sensor has been rinsed thoroughly with de-ionized water for three times. Then the sensor has been incubated with antibody for 1 h followed by washing with phosphate buffer saline (PBS). Fig. 2 (a) and (b) shows the top view SEM images of nanogrids on NPSO performed before and after immobilization of antibody using ZEISS, with an operating voltage of 20 kV and magnification of 100K. The wavy nature of graphene may be attributed to the fact that it follows the surface morphology of the template. The dimension of the pore before antibody immobilization is around 30 nm and the gap between them is around 35 nm. It is also evident that after functionalization by antibodies, the pore diameter reduces to 10 nm. The Fourier transform infrared (FTIR) spectra of the graphene sample before and after antibody functionalization are shown in Fig.2(c) and (d) respectively and have been recorded by the IR Affinity-1, SHIMADZU, Spectrophotometer in the mid IR range of 500-4000 cm^{-1} in kBr medium. The IR spectrum of graphene nanogrids shows the bands around 2800 and 2900 cm^{-1} due to symmetric and asymmetric stretching of C-H bonds. The peaks due to C=C, C-O and OH are present around 1600, 1000 and 3350 cm^{-1} respectively. From these findings, it is evident that sp^2 character is significantly enhanced for graphene nanogrids. After antibody attachment, the spectra show two prominent peaks around 1500 and 1600 cm^{-1} which is typical for monoclonal antibodies [32].The binding density of antibodies has also been obtained using UV VIS spectrophotometer (Perkin Elmer), following the methodology reported previously[33].The absorbance spectra obtained from the antibody coated graphene sensor surface has been represented in Fig.2(e). The existence of peak absorbance at around 280 nm confirms the presence of antibodies. From the calibration data of the instrument, the number of immobilized antibody molecules on the sensor surface has been found out to be of the order of 10^{11}.

To enclose the active region of the sensor, a PDMS well of approximately 2.5 mm thickness has been positioned in the region between the electrodes by observing under an optical microscope (Leica DM 2500). The width of the PDMS sheet is around 4 mm on all the sides. The PDMS sheets made from SYLGARD 184A and SYLGARD 184B has been obtained from Department of Chemical Engineering, IIT Kharagpur. For proper sealing of the PDMS with silicon oxide substrate, oxygen plasma treatment has been done [34]. Polyethylene tubing has been attached as the inlet and outlet of the PDMS wells through which proteins and buffer solutions have been drawn using a syringe pump. The protocol for antibody immobilization has been optimized in previous reports [33].

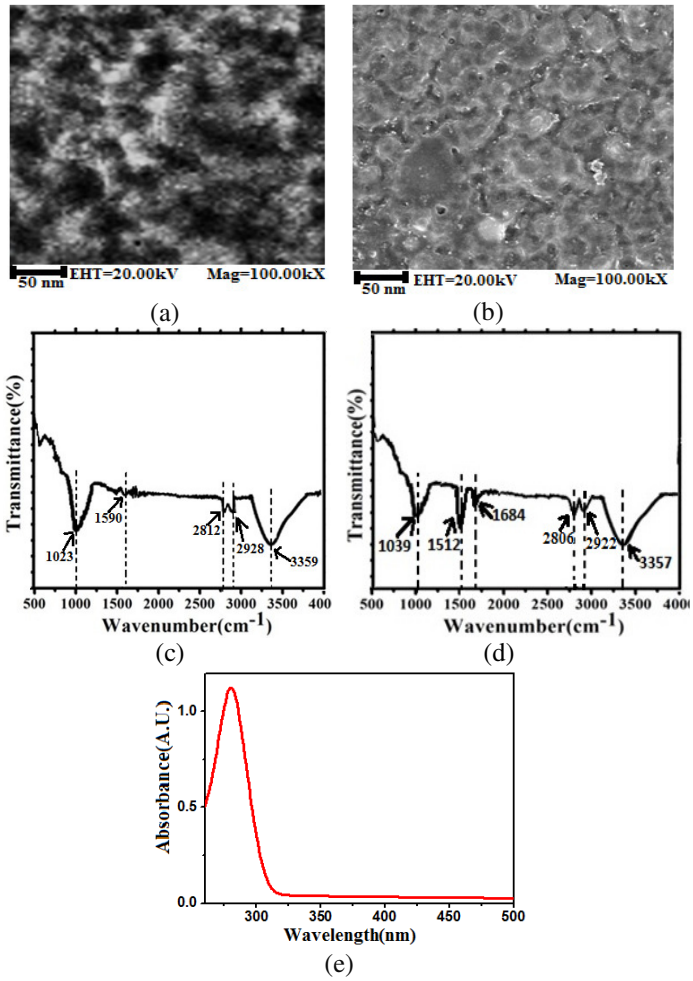

Fig.2 SEM image (top view) of grapheme nanogrids after (a) oxidation and (b) antibody attachment , FTIR spectra of the graphene sensor (c)before and (d) after antibody attachment (e) Absorption spectra after antibody attachment

C. Data Acquisition

Each sensor chip has been interfaced with the PC through a sensor holder set up. In the setup, the bond pads of the sensors have been placed below the probes of the sensor holder. The probes of the sensor holder which are in contact with the drain and source electrodes are spring loaded and adjustment screws have been provided to align them with the bond pads. The gate electrode has been inserted through a small hole in the setup and soldered to a metal connector. The picture of the setup is shown in Fig.3. Measurement has been performed in two steps. Firstly, buffer solution has been pumped through the

inlet at a flow rate of 130µl/min and after it has stabilized, the pump has been switched off and the electrical reading has been recorded as a function of time. Under this situation, the inlet and outlet tubings are both filled with buffer. Then 20 µl of analyte, i.e. serum has been injected at the inlet using the same pump at the rate of 2.5 µl/min. The analyte now diffuses towards the sensor surface and the electrical readings have been recorded in real time to identify the presence of specific molecules.

The gate electrode has been connected to a dc power supply (Keysight technologies). A high frequency signal of 20 mV amplitude in the range of 100 kHz to 1000 kHz has been applied through a signal generator (Agilent 33521A).It has been modulated by a reference signal of 1.43 kHz using a lock-in amplifier(Stanford Research, SR 830) and fed to the graphene FET at the source. The root mean square value of the mixing current (I_{mix}) through the drain terminal has been detected at the modulated frequency for a total duration of around 30 minutes, using the PC interface of the lock-in amplifier both before and after application of the analyte. Online computational analysis has been carried out in the same PC with MATLAB software for data analysis. The total analysis process has been divided in two phases: the calibration phase and testing phase. In the calibration phase, sensitivity of $I_{mix}(S)$ has been evaluated for various concentrations of the target antigen and then processed. In the testing phase, the unknown sensitivity value has been correlated with the concentration of the target antigen.

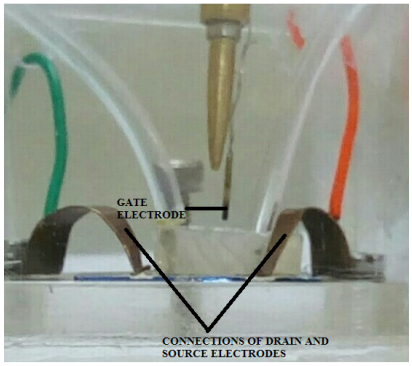

Fig.3 Picture of setup

D. Preparation of Virus Samples

Hep- B surface antigen has been used as the target molecule which has been procured from US Biological, USA (1 mg/ml).For the purpose of calibration, serial dilutions of Hep-B antigen solution has been performed in PBS with pH 7.2 and 100 mM ionic strength to produce concentrations ranging from 0.1fM to 1 pM of Hep-B. For measurements in physiological analyte, Hep-B surface antigen has been spiked in blood serum. The blood samples collected from a microbiological laboratory have been kept for some time at room temperature to separate the serum. The concentration of Hep-B has been limited to 1 pM, since the current output saturates for a higher concentration. For calibration of the sensor and generation of training data, 14 different concentrations of Hep-B surface antigen have been prepared. For each of these samples, 10 sensors have been fabricated. Thus, in a single batch, around 140 sensors have been developed. As measurement has been carried out in five batches, overall 700 sensors have been fabricated for the training. Mean and standard deviations have been recorded, both inter and intra batches. For testing with unknown solutions, different set of five sensors for each of them have been used and the mean sensitivities have been considered as inputs to the data processing software.

E. Data processing

The standard techniques used for quantification in most of the biochemical sensors is curve fitting. This has been implemented with the sensor characteristics and the error in quantification has been estimated. Further the data has also been processed by a static neural network. In the static model, a single neural network with tan hyperbolic activation function has been used. Finally to take into account the effect of data overlap and also incorporate the inherent drift of the sensors, PNN model has been developed. In the PNN model,/ data has been initially classified, depending on the single input parameter, sensitivity. This parameter has been first processed by a classifier neural network which converts it into a Dirac-Delta vector [30] of number of variables equal to that of the classes with corresponding class element for a certain class equal to 1 and the rest equal to 0. For example, if an input belongs to class 2 [indexing from 0], then the Dirac-Delta output vector for that input point would be [0 0 1 0 0 0 0 0 0 0 0 0 0 0 0]. This network consists of 2 hidden layers, having number of neurons equal to number of classes in each layer with probabilistic tan-hyperbolic activation function. In the output layer of this network, a *softmax* activation function has been trained with the data with *categorical-crossentropy* as the loss function and *Adam* optimizer. This is required so that the modulus of the Dirac-Delta output vector remains 1. This network helps to classify the regions with a significant overlap with an appreciable accuracy by probabilistically selecting the class for an input in the overlapped region over 50 iterations.

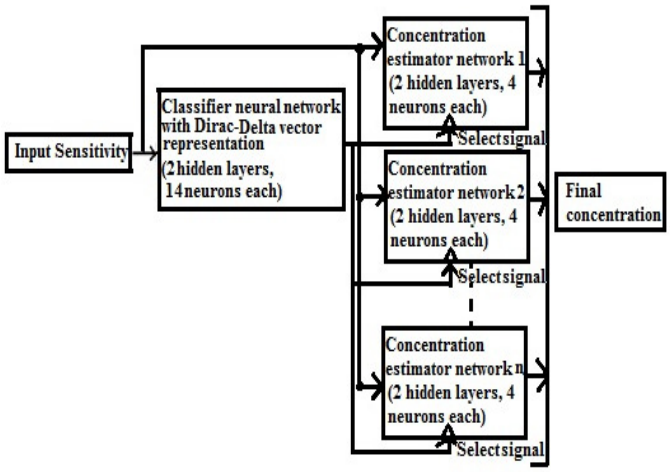

Fig.4 Scheme of the PNN model

This is followed by concentration estimator system which comprise of disjoint neural networks for the individual classes. These take the sensitivity value (normalized to 1) and the class (output of the classifier) to predict the concentration value. Each network in this block has been dedicated to a certain class and comprises of 2 hidden layers with 4 neurons in each,

running a probabilistic tan-hyperbolic function. Since these are also probabilistic networks, the output is generated over a certain number of iterations. The scheme of the PNN model is represented in Fig.4. This model has been trained with the sensor data obtained from the training solutions. For testing, the same model has been applied to the outputs of the test sensors which are different from that of the training sensors. As sensitivity is the input parameter, which has been calculated as the fractional change in I_{mix}, the deviation in the baseline value of I_{mix} between the training and test sensors do not interfere with the prediction.

F. Statistical Estimate

For validation of the developed sensor along with the data processing, the unknown samples have been tested by gold standard method using Hepatitis B surface antigen ELISA kits (US Biological H1909-09).As the graphene nanogrid sensor along with PNN is being validated for the first time, the sample size (n) has been estimated based on anticipated sensitivity (S_N) and specificity (S_P) [35] according to equation 1:

$$n\ based\ on\ sensitivity = \frac{Z^2_{1-\alpha/2} x S_N x (1-S_N)}{L^2 x\ Prevalence} \quad (1a)$$

$$n\ based\ on\ specificity = \frac{Z^2_{1-\alpha/2} x S_P x (1-S_P)}{L^2 x\ (1-Prevalence)} \quad (1b)$$

where *1-α* is the confidence level, $z_{1-\alpha/2}$ is the standard normal deviate corresponding to the specified size of the critical region (α) and L is the absolute precision desired on either side of sensitivity or specificity. For a 95% confidence level, 97% sensitivity and specificity, 0.1 as L and 0.6 as prevalence, n may be approximated to be 30 [35]. Thus, we have prepared 15 test samples with spiked Hep-B in serum and 15 samples have been considered as blank serum without the presence of any Hep-B surface antigen. The results obtained from the sensor system have been evaluated statistically in comparison to the gold standard by calculating the intra-class correlation coefficient and the proportionate bias.

III. Results and Discussions

A. FET Measurements

In a biomolecule functionalized graphene nanogrid FET sensor, carrier transport occurs in parallel through confined spaces of nanowire like graphene on top of the surface and stepped nanowires of graphene through the pores [12]. The high sensitivity and low detection limit of such sensors can be attributed to three reasons: firstly, the transconductance of the graphene nanogrid being high, the increase in the carrier concentration per antigen molecule is considerable with a probable localization effect of the charge modulation after antigen capture within the corresponding quantum dots [36], secondly, within the nanopores, the interaction between the walls and the biomolecules increase remarkably due to the average shorter distance than a flat surface which statistically raises the charge transfer probability per molecule and thirdly high receptor binding sites are available due to the increased surface area. At dc or low frequency, ions in solution can follow the variation of the electric field which results in formation of electric double layer for adequate screening. However at high frequencies, the ions experience a lag due to their finite diffusivity and hence do not have sufficient time to form the electric double layer. Under such circumstance, the first and second adsorbed water layers at the interface undergo molecular relaxation which weakens the electric double layer formation leading to higher penetration of ac electric field into the solution and hence the charged target molecules can modulate the surface potential of the graphene layer. At high frequency, the surface bound biomolecules behave as oscillating dipoles which modulate the local gate potential and thus, the change in generated current δI_{mix} is obtained from equation 2a[14]:

$$\partial I_{mix} = \gamma \frac{m}{2} \varphi cos\theta G \quad (2a)$$

where m is the modulation depth for the signal applied at the drain-source terminal, G is the transconductance of the sensor which can be calculated from the experimental characteristics of Fig.5a, γ represents the attenuation factor at the molecular dipole site with a phase lag of θ, given by equations 2b and 2c respectively:

$$\gamma = \frac{\sigma}{\sqrt{\sigma^2+4}},\ \sigma = \frac{\omega d \lambda}{D} \quad (2b)$$

$$\theta = tan^{-1}\frac{2}{\sigma} \quad (2c)$$

where ω is the applied frequency, d is the separation between the top gate electrode and the sensor surface, D is the diffusion coefficient of the ions in the buffer and λ is the Debye length. φ is the gating potential due to the dipoles given by equation 2d:

$$\phi = \frac{2[A]P}{4\pi\epsilon h} \quad (2d)$$

where *[A]* is the number of antigen molecules that get captured, P is the dipole moment corresponding to each antibody-antigen pair, ε is the dielectric constant and h is the distance between the antigen and the sensor surface.

Fig.5a shows the variation of drain to source current (I_{mix}) with gate to source voltage (V_{GS}) at different frequencies for drain to source voltage (V_{DS}) of 20mV in the graphene nanogrid device. The lower I_{mix} for positive V_{GS} indicates that the graphene sensor is primarily p-type. Fig.5b represents the variation of δI_{mix} with frequency after capture of 0.1 fM Hep-B in buffer. It has been observed that δI_{mix} is positive after the capture of Hep-B surface antigen. This may be attributed to the fact that Hep-B surface antigen is negatively charged at pH of 7.2 [37], leading to an increase in the carrier concentration and hence the conductivity. It has also been observed experimentally from Fig.5b that δI_{mix} after Hep-B capture increases with frequency since the weaker double layer leads to smaller θ and higher γ. Further, δI_{mix} increases significantly up to 1 MHz after which it remains almost constant and then it decreases. To explain this behavior, we have attempted to extract the values of δI_{mix} with frequency from equation 1. After application of 0.1 fM Hep-B, the number of antigen molecules that get captured*([A])* can be estimated from Langmuir equation 3:

$$[A] = \frac{C}{K_D}[Ab] \quad (3)$$

This article has been accepted for publication in a future issue of this journal, but has not been fully edited. Content may change prior to final publication. Citation information: DOI 10.1109/TNB.2018.2863734, IEEE Transactions on NanoBioscience

where C is the concentration of the analyte and K_D is the dissociation constant[38]. Considering a value of K_D of 1 nM and the number of bound antibodies ($[Ab]$) to be 10^{11} (from Sec.IIB), the total number of Hep-B captured is 10^4. h may be estimated from the SEM images of Fig.2(a) and (b). It has been observed that the effective diameter reduces by 20 nm which indicates that h may be considered to be 10 nm. ε may be assumed to be around $78\varepsilon_0$ for buffer, m has been maintained at 0.78, D has been assumed to be $10^{-9}m^2/s$, P has been approximated as 15.32 D [39] (the actual estimation of P for Hep-B surface antigen-antibody pair requires detailed molecular dynamics simulation and is beyond the scope of this paper) and d has been considered to be 500 nm. The theoretical variation of δI_{mix} with frequency after capture of antigen has also been plotted in Fig.5b. It has been observed that the trend is similar to that of the experiments but the value deviates owing to the approximation in the parameters. However, δI_{mix} shows a plateau after 5MHz theoretically. The experimental presence of a plateau at 1MHz followed by a decrease after 5MHz may be attributed to some resonance lost from measurement setup.

In a graphene FET sensor, it is necessary to eliminate any change in I_{mix} due to non-specific charges, like those which may be trapped at the interface of the sensor and from non-specific adsorption of biomolecules in serum. To reduce the interference from the non-specific charges at the interface of graphene and the functionalization layer, V_{gs} has been cycled ten times from -30 V to +30 V in presence of 100 mM PBS, initially at a frequency of 100 kHz. It has been observed that after 7 cycles, there is no further change in the transfer characteristics. The sensor has then been tested for stability at other frequencies of 200 kHz, 400 kHz, 600 kHz, 800 kHz, 1 MHz, 2 MHz and 5 MHz. It has been observed that for all these frequencies, the I_{mix}-V_{gs} characteristics become stable within the first three cycles. The steady characteristics have also been represented as a function of time in Fig.5c. It has been observed that at any frequency, I_{mix} remains almost steady in absence of any specific molecule. To confirm that the non-specific adsorption from serum does not interfere, we have also performed time dependent measurements of I_{mix} after injecting serum only, without any presence of Hep-B. It has been observed from Fig.5c that there is initially a shift in the baseline value but it returns to the original state after a period of approximately 100 seconds. This confirms that the change in I_{mix} is specific and is caused by the presence of Hep-B surface antigen in serum. It has also been observed that the time taken to achieve steady state is independent of the applied frequency and sensitivity increases with higher frequency. In Fig.5d, the variations of sensitivity after steady state has reached, has been plotted from the fractional change in I_{mix} for different concentrations of Hep-B in buffer and serum at the optimized frequency of 1 MHz. The sensitivity has decreased from that in buffer which is obvious since for the same amount of pippetted solution, lesser number of target molecules is captured. It is further observed that the deviation in sensitivity is significantly high in serum compared to that in buffer, especially for concentration of Hep-B less than 100 fM. This leads to overlap of sensitivity values which make it difficult to quantify the antigen in this range.

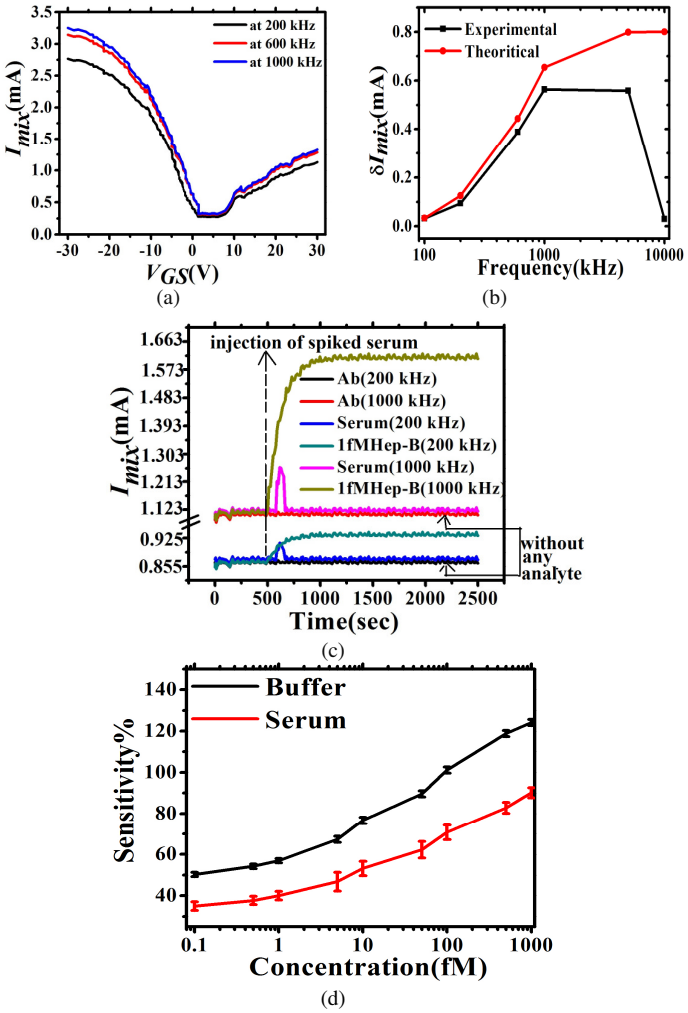

Fig.5(a) variation of I_{mix} with V_{GS} at different frequencies for V_{DS} of 20mV (b) Variation of $\delta Imix$ with frequency after Hep-B capture (c) Variation of I_{mix} with time after Hep-B capture in serum (d) The variations of sensitivity with concentrations in buffer and serum after steady state has reached

Table I indicates the mean sensitivity and its deviation, both inter and intra batches for different concentrations of Hep-B in serum at 1 MHz. The data corresponding to Table I have been represented in the form of a graph in Fig.6. It may be inferred from Fig.6 that there is a significant overlap between the different concentration ranges.The reason for this significant overlap is that for the same quantity of target antigen in serum, the number of captured antigen is different during real time detection, since the concentration of non-target antigen in serum is many times higher than the target antigen. For non-real time detection, usually the total analyte is exposed to the sensor surface, instead of flowing it through the channels, which is then followed by washing steps. This reduces the variation in the number of captured antigen, even in serum and hence the overlap and the corresponding drift. Impedance biosensors on nanostructured silicon oxide had been reported to exhibit some degree of overlap in the sensitivities for complex solution, during non-real time operation [21-23]. The problem had been addressed by incorporating a second parameter. However, for graphene FET biosensor, the only input parameter is sensitivity. Hence probabilistic features

need to be included in the signal processing to address the uncertainties due to the inherent drift.

TABLE-I
SENSITIVITY VALUES FOR DIFFERENT ANTIGEN CONCENTRATION

Concentration of Hep-B (fM)	Mean sensitivity and its range (%)	Deviation of man sensitivity between batches (%)
0.1	35, 32.9-37.01	5.85
0.25	37,34.9-39.13	6.2
0.5	38, 36.95-39.2	5.7
0.75	38.5,37.9-39.2	5.2
1	39, 38.5-39.52	6.1
2.5	42, 38.8-45.2	4.5
5	44.7, 39-50.34	3.9
10	49,45.8-52.2	4.1
25	51, 50.5-51.5	3.5
50	60, 50.9-70.1	4.3
100	70, 58.8-81.1	5.2
250	75, 67.7-82.3	3.2
500	82.5, 79.7-85.35	3.6
1000	90.25, 88.5-95	3.2

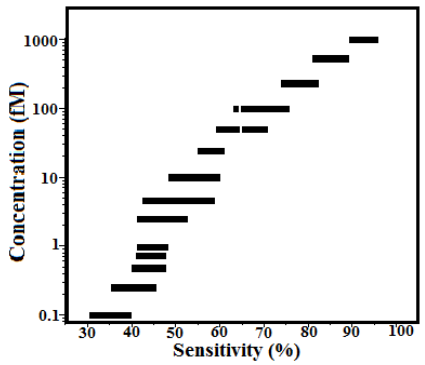

Fig.6 Representation of the data in the form of graph corresponding to Table I

B. *Polynomial fitting and static neural networks*

It has been observed from Table I that majority of the values reside in lower concentration range. As any standard curve fitting model tries to minimize the overall error, better accuracy is obtained at higher concentration than the lower range. Moreover such fitting ignores the overlap zones. It has been observed that the mean square error saturates after 6th degree. In a static neural network model, the training has been continued until mean square error reduced to an acceptable range. As the lower concentration is not prioritized, this range suffers from a large deviation from the actual value. Table II represents the outputs from the polynomial fit and the static neural network model for 15 different test solutions. Each solution has been tested with five sensors and the mean sensitivity has been considered as the input. It has been observed that the maximum error is as high as around 77% and 66% with polynomial fit and static neural network model respectively.

TABLE-II
OUTPUT OF POLYNOMIAL FIT AND SINGLE LAYER NEURAL NETWORK

Sensitivity (%)	Polynomial (Deg. 6) (fM)	Single Layer Neural Network Model (fM)	Output from gold standard (fM)
33.2	0.07	0.25	0.15
34.5	0.1	0.3	0.2
35.2	0.12	0.45	0.3
38	0.09	0.6	0.4
38.5	1	1	0.6
39	1.1	0.7	0.8
39.4	1.3	1.4	1.5
39.6	1.8	1.85	2
42	2.2	3.8	3
43.4	3.5	4.5	4
45.2	4	6	8
50.5	10.1	20	15
50.9	11	28	20
53.9	50	48	35
64.6	98	50	70

C. *Probabilistic neural network model*

The probability in the data has been incorporated in the activation function of the hidden layer neurons, thus making the whole network dynamic. We use a probabilistic tan-hyperbolic activation function to achieve the intended goal as expressed in equation 4:

$$g(x) = f(q.x) = \frac{e^{qx} - e^{-qx}}{e^{qx} + e^{-qx}} \quad (4)$$

where q is a random variable from a chosen probability distribution. For a normal distribution with mean =1 and standard deviation as 10%, for 1000 iterations, the probabilistic nature is observed in Fig.7. The transparency in this figure is inversely proportional to the probability, i.e. higher the transparency, lower is the probability of that particular curve appearing. The probabilistic variations of the activation function in the classifier neural networks and the concentration estimator networks eventually result in the generation of a range of output concentrations for a particular input sensitivity. As the classifier neural network with two hidden layers having 14 neurons each, is a fully connected network, the number of learning parameters is 196. Again each of the concentration estimator block with two hidden layers having four neurons each, requires 16 learning parameters. For a total of 212 parameters, it is desirable to have training data, 10 times greater than learning parameters. However, as the number of training data are 700 (as mentioned in Sec.IID), we have generated intermediate data points in each class within the range indicated in Table I. To estimate the effect of the size of training data, we have generated 500 and 1000 data in each class, thus an overall training data of both 7000 and 14,000 have also been used. For each of the training data size, R^2 score has been computed from equation 5:

$$R^2 = 1 - \frac{SSE}{SST} \quad (5)$$

where SST and SSE are the sum of squared errors for a baseline model without any training and that of the final model after training respectively. Thus the worst possible value of R^2 is 0 and the best value is 1.

It has been observed that the R^2 score has not increased substantially when the training data set has been changed from 700 to 7000 to 14000, primarily because a probabilistic model has been used. Thus, the training data set has been finalized at

700.

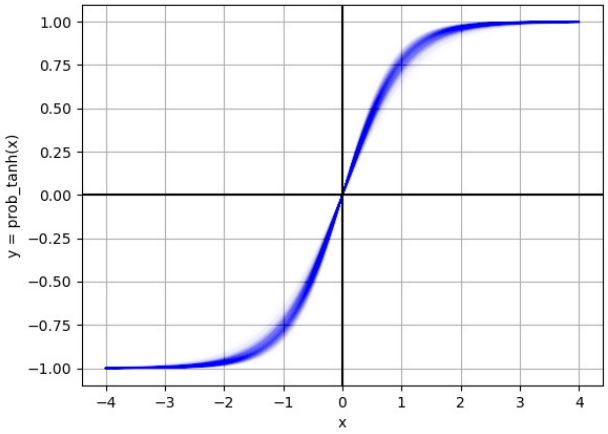

Fig.7 Probabilistic tan-hyperbolic function

The concentration estimator in Fig.4 has been iterated over 50 times and the mean output has been considered. The output of the PNN at every stage has been listed in Table III. It has been observed that for every input sensitivity, the classifier network selects either multiple classes or a single class (corresponding to the position of '1') during the iteration stages, depending on the overlapping nature of the input. The classes have been represented in Table III with decreasing probability. Each of the class invokes the corresponding concentration estimator network depending on the position of '1'and at the end of 50 iterations, a range of output has been obtained. The final output has been considered as the mean of this range which has been compared with the gold standard. The remaining 15 solutions with absence of any spiked Hep-B has been processed as negative since the sensitivities obtained were within 5% which is almost six times lower than the minimum sensitivity corresponding to 0.1 fM. The comparison in Table III clearly indicates the reduction in the maximum quantification error within 10%, even for the concentration range of 0.1 fM to 100 fM.

TABLE-III
OUTPUT OF PNN MODEL

Sensitivity (%)	Classifier Outputs (Decreasing Probability)	Concentration Estimator Network **Mean** and Range (fM)	Output from gold standard (fM)
33.2	[1 0 0 0 0 0 0 0 0 0 0 0 0 0 0 0] [0 1 0 0 0 0 0 0 0 0 0 0 0 0 0 0]	**0.16** 0.9-0.19	0.15
34.5	[0 1 0 0 0 0 0 0 0 0 0 0 0 0 0 0] [1 0 0 0 0 0 0 0 0 0 0 0 0 0 0 0]	**0.19** 0.12-0.24	0.2
35.2	[0 1 0 0 0 0 0 0 0 0 0 0 0 0 0 0] [1 0 0 0 0 0 0 0 0 0 0 0 0 0 0 0]	**0.32** 0.27-0.39	0.3
38	[0 0 1 0 0 0 0 0 0 0 0 0 0 0 0 0] [0 0 0 1 0 0 0 0 0 0 0 0 0 0 0 0]	**0.43** 0.38-0.50	0.4
38.5	[0 0 1 0 0 0 0 0 0 0 0 0 0 0 0 0] [0 0 0 1 0 0 0 0 0 0 0 0 0 0 0 0] [0 0 0 0 1 0 0 0 0 0 0 0 0 0 0 0]	**0.55** 0.49-0.67	0.6
39	[0 0 0 0 1 0 0 0 0 0 0 0 0 0 0 0] [0 0 0 0 0 1 0 0 0 0 0 0 0 0 0 0]	**0.75** 0.64-0.92	0.8
39.4	[0 0 0 0 1 0 0 0 0 0 0 0 0 0 0 0]	**1.62**	1.5
	[0 0 0 0 0 1 0 0 0 0 0 0 0 0 0 0]	1.23-1.86	
39.6	[0 0 0 0 0 0 1 0 0 0 0 0 0 0 0 0] [0 0 0 0 1 0 0 0 0 0 0 0 0 0 0 0] [0 0 0 0 0 1 0 0 0 0 0 0 0 0 0 0]	**1.9** 1.74-2.32	2
42	[0 0 0 0 0 0 1 0 0 0 0 0 0 0 0 0] [0 0 0 0 0 0 0 1 0 0 0 0 0 0 0 0]	**3.3** 2.56-3.87	3
43.4	[0 0 0 0 0 0 0 1 0 0 0 0 0 0 0 0] [0 0 0 0 0 0 0 0 1 0 0 0 0 0 0 0]	**4.3** 3.9-5.12	4
45.2	[0 0 0 0 0 0 0 0 1 0 0 0 0 0 0 0] [0 0 0 0 0 0 0 0 0 1 0 0 0 0 0 0]	**8.6** 7.78-9.2	8
50.5	[0 0 0 0 0 0 0 0 0 0 0 0 1 0 0 0]	**14.7** 12.63-16.19	15
50.9	[0 0 0 0 0 0 0 0 0 0 0 0 0 1 0 0] [0 0 0 0 0 0 0 0 0 0 0 0 1 0 0 0]	**18.5** 16.8-20.5	20
53.9	[0 0 0 0 0 0 0 0 0 0 0 0 0 0 1 0]	**37** 34.44-40.93	35
64.6	[0 0 0 0 0 0 0 0 0 0 0 0 0 0 0 1] [0 0 0 0 0 0 0 0 0 0 0 0 0 0 1 0]	**73** 64.64-81.3	70

D. *Statistical Analysis of Data*

The intra-class correlation coefficient for agreement of quantification of Hep-B surface antigen between our method and gold standard method is 0.953**,** p<0.001 which denotes an excellent agreement between the two measures in our study sample. The 95% CI ranges from 0.801 to 0.989 signifying a good to excellent agreement when extrapolated to the population, as shown in Table IV.

TABLE-IV
INTRA-CLASS CORRELATION COEFFICIENT- CONTROL GROUP: AGREEMENT FOR QUANTIFICATION OF HEP-B ANTIGEN BETWEEN PROPOSED METHOD AND GOLD STANDARD METHOD

		95% Confidence Interval		F Test with True Value 0			
Measures	Intraclass Correlation[b]	Lower Bound	Upper Bound	Value	df1	df2	p
Single Measures	.910[a]	.668	.979	20.031	8	8	<0.001
Average Measures	.953[c]	.801	.989	20.031	8	8	<0.001

Two-way mixed effects model where people effects are random and measures effects are fixed.

a. The estimator is the same, whether the interaction effect is present or not.

b. Type A intra-class correlation coefficients using an absolute agreement definition.

c. This estimate is computed assuming the interaction effect is absent, because it is not estimable otherwise.

A regression model analysis has also been executed to determine the coefficient of regression with difference in quantification of Hep-B surface antigen detection response between the two methods as dependent variable and average detection response of the two methods as independent variable. We have obtained a non-significant p value (p=0.051) in the model indicating that there is no proportional bias in the model, as presented in Table V. It means they have good agreement in both higher and lower values.

TABLE-V
REGRESSION COEFFICIENTS – CONTROL GROUP

Model		Unstandardized Coefficients		Standa-rdized Coeffi-cients	t	Sig.
		B	Std. Error	Beta		
Final Step	(Constant)	68.818	27.466		2.506	0.041
	Average Hep-B Antigen quantitati-ve response	-0.299	0.126	-0.669	-2.38	0.051

a. Dependent Variable: Diff Hep-B Antigen quantitative response

The performance has been compared with existing reports of real time and label free specific biomolecule detection in physiological analyte using graphene and other sensors. It is observed from Table VI that using graphene, the proposed methodology provides an improvement by three orders of magnitude and compared to other sensor for Hep-B detection, the present technique lowers the detection limit by more than three orders of magnitude. This is extremely desirable for practical implementation. After the onset of Hep-B virus infection, Hep-B surface antigen is found in abundance in serum. Most of the existing commercial assays suffer from low sensitivity with detection limits of few nM. At this concentration, the infection has already progressed and condition becomes critical. To overcome this problem, the development presented in this paper will result in significantly accurate quantification of Hep-B surface antigen down to 0.1 fM in serum. This will enable early detection of Hep-B infection which eventually will reduce the treatment cost.

TABLE-VI
COMPARISON WITH OTHER REPORTS IN SERUM

Reference	Substrate/Target molecules	Limit of Detection	Range
17	Graphene, prostate specific antigen	1 nM	1000 nM
18	Graphene ,Native Zika virus antigen	450 pM	450 nM
19	Graphene ,Brain natriuretic peptide	100 fM	100 pM
20	Graphene ,Lead ions	0.1 ng/ml	1 ng/ml
40	, Hep-B surface antigen	400 fM	400 pM
This report	Graphene nanogrids, Hep-B surface antigen	0.1 fM	1 pM

IV. CONCLUSION

This paper successfully demonstrates the quantification of Hep-B surface antigen in serum down to 0.1 fM, during real time operation by applying PNN on graphene nanogrids FET biosensor. The error in detection has been reduced within 10% which is an improvement by around 85% compared to polynomial fit and static neural network model. The presented method has resulted in lowering of the detection limit by more than three orders of magnitude compared to the state-of-art sensors for Hep-B detection, hence enhancing the potential of graphene FET towards clinical diagnostics. The signal processing approach may be extended to other biochemical sensors for label free, real time and ultrasensitive biomolecule detection.

ACKNOWLEDGEMENT

The authors would like to acknowledge Dr.Ramkrishna Dev Das of Saha Institute of Nuclear Physics for the Raman characterization and Prof. H.Saha of Center of Excellence for Green Energy and Sensor Systems for surface profilometry studies.

REFERENCES.

[1] J. Li, S. Pud, M. Petrychuk, A. Offenhäusser, and S. Vitusevich, "Sensitivity Enhancement of Si Nanowire Field Effect Transistor Biosensors Using Single Trap Phenomena," *Nano Letters*, vol. 14, no. 6, pp. 3504–3509, 2014.

[2] N. Aroonyadet, X. Wang, Y. Song, H. Chen, R. J. Cote, M. E. Thompson, R. H. Datar, and C. Zhou, "Highly Scalable, Uniform, and Sensitive Biosensors Based on Top-Down Indium Oxide Nanoribbons and Electronic Enzyme-Linked Immunosorbent Assay," *Nano Letters*, vol. 15, no. 3, pp. 1943–1951, 2015.

[3] H. Ghosh and C. Roychaudhuri, "Ultrasensitive food toxin biosensor using frequency based signals of silicon oxide nanoporous structure," *Applied Physics Letters*, vol. 102, no. 24, p. 243701, 2013.

[4] C. S. Martinez-Cisneros, S. Sanchez, W. Xi, and O. G. Schmidt, "Ultracompact Three-Dimensional Tubular Conductivity Microsensors for Ionic and Biosensing Applications," *Nano Letters*, vol. 14, no. 4, pp. 2219–2224, 2014.

[5] J.-H. Han, D. Lee, C. H. C. Chew, T. Kim, and J. J. Pak, "A multi-virus detectable microfluidic electrochemical immunosensor for simultaneous detection of H1N1, H5N1, and H7N9 virus using ZnO nanorods for sensitivity enhancement," *Sensors and Actuators B: Chemical*, vol. 228, pp. 36–42, 2016.

[6] S. Guo, D. Wen, Y. Zhai, S. Dong, and E. Wang, "Platinum Nanoparticle Ensemble-on-Graphene Hybrid Nanosheet: One-Pot, Rapid Synthesis, and Used as New Electrode Material for Electrochemical Sensing," *ACS Nano*, vol. 4, no. 7, pp. 3959–3968, 2010.

[7] V. Gupta, "ZnO based third generation biosensor," *Thin Solid Films*, vol. 519, no. 3, pp. 1141–1144, 2010.

[8] T. Bertok, A. Sediva, A. Vikartovska, J.Tkac, "Comparison of the 2D and 3D nanostructured lectin-based biosensors for In Situ detection of sialic acid on glycoproteins," , *Int. J. Electrochem. Sci*., vol. 9, no. 2, pp.890-900, 2014.

[9] C. Xue, C.-C. Kung, M. Gao, C.-C. Liu, L. Dai, A. Urbas, and Q. Li, "Facile fabrication of 3D layer-by-layer graphene-gold nanorod hybrid architecture for hydrogen peroxide based electrochemical biosensor," *Sensing and Bio-Sensing Research*, vol. 3, pp. 7–11, 2015.

[10] Y. Li, R. Zhao, L. Shi, G. Han, and Y. Xiao, "Acetylcholinesterase biosensor based on electrochemically inducing 3D graphene oxide network/multi-walled carbon nanotube composites for detection of pesticides," *RSC Advances*, vol. 7, no. 84, pp. 53570–53577, 2017.

[11] B.-Y. Kim, I.-Y. Sohn, D. Lee, G. S. Han, W.-I. Lee, H. S. Jung, and N.-E. Lee, "Ultrarapid and ultrasensitive electrical detection of proteins in a three-dimensional biosensor with high capture efficiency," *Nanoscale*, vol. 7, no. 21, pp. 9844–9851, 2015.

[12] J.Basu, and C.RoyChaudhuri, "Attomolar sensitivity of FET biosensor based on smooth and reliable graphene nanogrids" *IEEE Electron Device Lett,* vol. 37, no. 4, pp. 492-495, 2016.

[13] O. Akhavan, E. Ghaderi, and R. Rahighi, "Toward Single-DNA Electrochemical Biosensing by Graphene Nanowalls," *ACS Nano*, vol. 6, no. 4, pp. 2904–2916, 2012.

[14] G. S. Kulkarni and Z. Zhong, "Detection beyond the Debye Screening Length in a High-Frequency Nanoelectronic Biosensor," *Nano Letters*, vol. 12, no. 2, pp. 719–723, 2012.
[15] C.-H. Chu, I. Sarangadharan, A. Regmi, Y.-W. Chen, C.-P. Hsu, W.-H. Chang, G.-Y. Lee, J.-I. Chyi, C.-C. Chen, S.-C. Shiesh, G.-B. Lee, and Y.-L. Wang, "Beyond the Debye length in high ionic strength solution: direct protein detection with field-effect transistors (FETs) in human serum," *Scientific Reports*, vol. 7, no. 1, pp. 5256(1-15), 2017.
[16] N. Gao, W. Zhou, X. Jiang, G. Hong, T.-M. Fu, and C. M. Lieber, "General Strategy for Biodetection in High Ionic Strength Solutions Using Transistor-Based Nanoelectronic Sensors," *Nano Letters*, vol. 15, no. 3, pp. 2143–2148, 2015.
[17] N. Gao, T. Gao, X. Yang, X. Dai, W. Zhou, A. Zhang, and C. M. Lieber, "Specific detection of biomolecules in physiological solutions using graphene transistor biosensors," *Proceedings of the National Academy of Sciences*, vol. 113, no. 51, pp. 14633–14638, 2016.
[18] S. Afsahi, M. B. Lerner, J. M. Goldstein, J. Lee, X. Tang, D. A. Bagarozzi, D. Pan, L. Locascio, A. Walker, F. Barron, and B. R. Goldsmith, "Novel graphene-based biosensor for early detection of Zika virus infection," *Biosensors and Bioelectronics*, vol. 100, pp. 85–88, 2018.
[19] Y.-M. Lei, M.-M. Xiao, Y.-T. Li, L. Xu, H. Zhang, Z.-Y. Zhang, and G.-J. Zhang, "Detection of heart failure-related biomarker in whole blood with graphene field effect transistor biosensor," *Biosensors and Bioelectronics*, vol. 91, pp. 1–7, 2017.
[20] C. Wang, X. Cui, Y. Li, H. Li, L. Huang, J. Bi, J. Luo, L. Q. Ma, W. Zhou, Y. Cao, B. Wang, and F. Miao, "A label-free and portable graphene FET aptasensor for children blood lead detection," *Scientific Reports*, vol. 6, no. 1, pp. 21711, 2016.
[21] H. Ghosh and C. Roychaudhuri, "Noise spectroscopy as an efficient tool for impedance based sub-femtomolar toxin detection in complex mixture using nanoporous silicon oxide," *Biosensors and Bioelectronics*, vol. 67, pp. 757–762, 2015.
[22] H. Ghosh, R. Das, and C. Roychaudhuri, "Optimized Nanocrystalline Silicon Oxide Impedance Immunosensor Electronic Tongue for Subfemtomolar Estimation of Multiple Food Toxins," *IEEE Transactions on Instrumentation and Measurement*, vol. 66, no. 5, pp. 964–973, 2017.
[23] N. Samanta and C. Roychaudhuri, "Nanocrystalline Silicon Oxide Impedance Immunosensors for Sub-Femtomolar Mycotoxin Estimation in Corn Samples by Incremental Fuzzy Approach," *IEEE Sensors Journal*, vol. 16, no. 4, pp. 1069–1078, 2016.
[24] A. Ghosh, P. Sharma, B. Tudu, S. Sabhapondit, B. D. Baruah, P. Tamuly, N. Bhattacharyya, and R. Bandyopadhyay, "Detection of Optimum Fermentation Time of Black CTC Tea Using a Voltammetric Electronic Tongue," *IEEE Transactions on Instrumentation and Measurement*, vol. 64, no. 10, pp. 2720–2729, 2015.
[25] L. Lvova, C. G. Branchini, K. Petropoulos, L. Micheli, G. Volpe, E. Viaggiu, R. Congestri, L. Guzzella, F. Pozzoni, C. D. Natale, and R. Paolesse, "E-tongue for Ecological Monitoring Purposes: The Case of Microcystins Detection," *Procedia Engineering*, vol. 87, pp. 1358–1361, 2014.
[26] J. Y. Heras, D. Pallarola, and F. Battaglini, "Electronic tongue for simultaneous detection of endotoxins and other contaminants of microbiological origin," *Biosensors and Bioelectronics*, vol. 25, no. 11, pp. 2470–2476, 2010.
[27] Z. Liu and H.-X. Li, "A probabilistic fuzzy logic system for modeling and control," *IEEE Transactions on Fuzzy Systems*, vol. 13, no. 6, pp. 848–859, 2005.
[28] M. K. Morris, J. Saez-Rodriguez, D. C. Clarke, P. K. Sorger, and D. A. Lauffenburger, "Training Signaling Pathway Maps to Biochemical Data with Constrained Fuzzy Logic: Quantitative Analysis of Liver Cell Responses to Inflammatory Stimuli," *PLoS Computational Biology*, vol. 7, no. 3, pp. e1001099, 2011.
[29] "Pathway and network analysis of cancer genomes," *Nature Methods*, vol. 12, no. 7, pp. 615–621, 2015.
[30] W. Ford, K. Xiang, W. Land, R. Congdon, Y. Li, and O. Sadik, "A Multi-class Probabilistic Neural Network for Pathogen Classification," *Procedia Computer Science*, vol. 20, pp. 348–353, 2013.
[31] D. F. Specht, "Probabilistic neural networks," *Neural Networks*, vol. 3, no. 1, pp. 109–118, 1990.
[32] M. Boulet-Audet, S. G. Kazarian, and B. Byrne, "In-column ATR-FTIR spectroscopy to monitor affinity chromatography purification of monoclonal antibodies," *Scientific Reports*, vol. 6, pp. 30526, 2016.
[33] R. D. Das, S. Maji, S. Das, and C. Roychaudhuri, "Optimization of covalent antibody immobilization on macroporous silicon solid supports," *Applied Surface Science*, vol. 256, no. 20, pp. 5867–5875, 2010.
[34] D. Mondal, C. Roychaudhuri, L. Das, and J. Chatterjee, "Microtrap electrode devices for single cell trapping and impedance measurement," *Biomedical Microdevices*, vol. 14, no. 5, pp. 955–964, 2012.
[35] R. Malhotra and A. Indrayan, "A simple nomogram for sample size for estimating sensitivity and specificity of medical tests," *Indian Journal of Ophthalmology*, vol. 58, no. 6, pp. 519-522, 2010.
[36] P. Gallagher, K. Todd, and D. Goldhaber-Gordon, "Disorder-induced gap behavior in graphene nanoribbons," *Phys. Rev. B*, vol. 81, pp. 115409-1–115409-8, 2010.
[37] Y. Wang, K. Chen, Z. Wu, Y. Liu, S. Liu, Z. Zou, S.-H. Chen, and C. Qu, "Immunizations with hepatitis B viral antigens and a TLR7/8 agonist adjuvant induce antigen-specific immune responses in HBV-transgenic mice," *International Journal of Infectious Diseases*, vol. 29, pp. 31–36, 2014.
[38] B. Bose, D. A. Chugh, M. Kala, S. K. Acharya, N. Khanna, and S. Sinha, "Characterization and molecular modeling of a highly stable anti-Hepatitis B surface antigen scFv," *Molecular Immunology*, vol. 40, no. 9, pp. 617–631, 2003.
[39] J. Dechancie and K. N. Houk, "The Origins of Femtomolar Protein−Ligand Binding: Hydrogen-Bond Cooperativity and Desolvation Energetics in the Biotin−(Strept)Avidin Binding Site," *Journal of the American Chemical Society*, vol. 129, no. 17, pp. 5419–5429, 2007.
[40] M. S. Diware, H. M. Cho, W. Chegal, Y. J. Cho, S. W. O, S.-H. Paek, D. S. Kim, K.-S. Kim, Y. G. Min, J. H. Jo, and C. Shin, "Label-free detection of hepatitis B virus using solution immersed silicon sensors," *Biointerphases*, vol. 12, no. 1, pp. 01A402, 2017.

Rohit Ray is currently pursuing his Integrated M.Tech in Electronics and Telecommunication Engineering Departme. He is working in the area of signal processing for biological applications.

Joyeeta Basu received her M.Tech degree from West Bengal University of Technology, India, in 2013 and currently pursuing Ph.D at IIEST in the field of graphene based electrical biosensors for virus detection.

Wasim Akram Gazi is currently with Qualcomm Technologies, Bangalore, India and his research interest is in the domain of biomedical signal pricessing and chip design.

Nirmalya Samanta received the M.Tech. degree the West Bengal University of Technology, India. He is currently pursuing the Ph.D. at IIEST, Shibpur, India in the development of signal processing system for biosensors.

Kingshuk Bhattacharyya is currently pursuing his research in the Department of Medical Sciences at JJT University Rajasthan. His research interest is statistical analysis of clinical data to obtain commercial perspectives.

Chirasree RoyChaudhuri (SM'13) is presently an Assistant professor in Department of Electronics and Telecomm. Engg., IIEST Shibpur, India. Her fields of research interest are development of selective electrical biosensors, understanding the physical mechanisms for sub-femtomolar detection, measurement of biophysical properties of cells through distributed models.